BBA - Biomembranes 1863 (2021) 183723

Contents lists available at ScienceDirect

BBA - Biomembranes

journal homepage: www.elsevier.com/locate/bbamem

Interactions of HIV gp41's membrane-proximal external region and transmembrane domain with phospholipid membranes from ^{31}P NMR

Madeleine Sutherland, Byungsu Kwon, Mei Hong *

Department of Chemistry, Massachusetts Institute of Technology, Cambridge, MA, USA

ARTICLE INFO

Keywords:
Cholesterol
Virus-cell fusion
Membrane curvature
Protein dynamics

ABSTRACT

HIV-1 entry into cells requires coordinated changes of the conformation and dynamics of both the fusion protein, gp41, and the lipids in the cell membrane and virus envelope. Commonly proposed features of membrane deformation during fusion include high membrane curvature, lipid disorder, and membrane surface dehydration. The virus envelope and target cell membrane contain a diverse set of phospholipids and cholesterol. To dissect how different lipids interact with gp41 to contribute to membrane fusion, here we use ^{31}P solid-state NMR spectroscopy to investigate the curvature, dynamics, and hydration of POPE, POPC and POPS membranes, with and without cholesterol, in the presence of a peptide comprising the membrane proximal external region (MPER) and transmembrane domain (TMD) of gp41. Static ^{31}P NMR spectra indicate that the MPER-TMD induces strong negative Gaussian curvature (NGC) to the POPE membrane but little curvature to POPC and POPC:POPS membranes. The NGC manifests as an isotropic peak in the static NMR spectra, whose intensity increases with the peptide concentration. Cholesterol inhibits the NGC formation and stabilizes the lamellar phase. Relative intensities of magic-angle spinning ^{31}P cross-polarization and direct-polarization spectra indicate that all three phospholipids become more mobile upon peptide binding. Finally, 2D ^{1}H-^{31}P correlation spectra show that the MPER-TMD enhances water ^{1}H polarization transfer to the lipids, indicating that the membrane surfaces become more hydrated. These results suggest that POPE is an essential component of the high-curvature fusion site, and lipid dynamic disorder is a general feature of membrane restructuring during fusion.

1. Introduction

At its height as an epidemic, HIV killed millions of people. Although anti-retroviral therapy has transformed HIV into a manageable chronic condition, drug resistance and adverse side effects motivate continued fundamental studies of essential HIV proteins. HIV entry into CD4^{+} T-lymphocytes and macrophages is mediated by the trimeric Env glycoprotein complex [1]. The gp120 component of the complex binds host cell CD4, CCR5 and CXCR4 receptors, and dissociates from gp41. Gp41 then proceeds to fuse the virus lipid envelope with the host cell membrane via a cascade of conformational changes [2,3]. This membrane fusion involves an initial merger of the outer leaflets of the virus and cell membranes, followed by fusion of the inner leaflets, and subsequently the emergence and enlargement of a water-filled pore that permits the virus particle to enter the cell [4]. This virus-cell fusion involves intermediate, energetically unfavorable structural changes of two lipid membranes and the intervening water layer, and it is only possible due to the energetically favorable conformational changes of the fusion protein from a metastable prefusion state to an equilibrium post-fusion state [5,6].

The protein-lipid structural changes involved in membrane fusion have been extensively studied, but many questions remain due to the conformational plasticity of these fusion complexes. On the protein side, gp41 transits through at least three conformational states: a prefusion state, an extended intermediate state where an N-terminal fusion peptide (FP) is inserted into the target cell membrane, and a post-fusion state. In the post-fusion state, the N- and C-terminal halves of the water-soluble portion of the protein are bent into a trimer of hairpins, pulling the target cell membrane and the virus envelope into close proximity [7]. Crystal structures of the prefusion and post-fusion states are known for gp41 and a number of other class I viral fusion proteins [8–11], while the intermediate states remain difficult to capture [12,13]. Although post-fusion structures of the ectodomain are available for many viral fusion proteins, their biological relevance is still unclear, as these structures are usually obtained in the absence of the transmembrane domain (TMD) [9]. Recent NMR studies of the C-terminal

* Corresponding author.
E-mail address: meihong@mit.edu (M. Hong).

https://doi.org/10.1016/j.bbamem.2021.183723
Received 30 April 2021; Received in revised form 22 July 2021; Accepted 30 July 2021
Available online 2 August 2021

region of gp41 that includes a membrane-proximal external region (MPER) and the TMD provided some of the missing information. In lipid bilayers that mimic the virus envelope, the MPER-TMD peptide forms trimers, with the MPER helix lying on the membrane surface while the TMD helix spanning the membrane [14] (Fig. 1). In DMPC:DHPC bicelles, the MPER-TMD also shows a trimeric assembly based on intermolecular paramagnetic relaxation enhancement NMR data [15], but the MPER conformation differs from that obtained in lipid bilayers. When only the TMD is incorporated into bicelles, both monomeric and trimeric structures have been reported using solution NMR [16,17], suggesting that the TMD structure might be sensitive to environmental effects such as peptide concentration, temperature, and bicelle size. In lipid bilayers, when the gp41 fusion peptide is covalently linked to the MPER-TMD in a chimera, no cross peaks were detected between the FP and TMD residues, indicating that the FP and TMD do not come into close molecular contact to form a helical bundle [18]. Therefore, these two hydrophobic ends of the protein, as engineered in the chimera, do not appear to form a tight six-helix bundle like the ectodomain. Similarly, a FP-TMD chimera of the parainfluenza virus 5 fusion protein F also does not exhibit correlation peaks between the FP residues and TMD residues [19]. These results open the question of how these N- and C-terminal hydrophobic domains restructure the lipid membrane to generate fusion intermediates and the fusion pore.

In addition to protein conformational changes, individual lipids need to interact with the proteins to incur membrane curvature and membrane dehydration during virus-cell fusion. Molecular details of these protein-lipid interactions are still poorly understood. The main curvature effect that is believed to occur during membrane fusion is the negative Gaussian curvature (NGC) (Fig. 1), where every point on a surface has opposite-signed principal curvatures [20,21]. NGC is known to be important in many membrane-remodeling events such as fusion, scission, and pore formation [21–24], and can be characterized using small-angle X-ray scattering and solid-state ^{31}P NMR. Lipids with intrinsic curvature tendencies in membranes such as phosphatidylethanolamine (PE) and lysophosphocholine (LPC) promote and inhibit protein-free membrane fusion, respectively [5], but how these lipids interact with proteins to mediate membrane fusion has not been studied. Biochemical data show that negatively charged phosphatidylserine (PS) and cholesterol are both cofactors in Env-mediated HIV-cell fusion. The virion envelope and the target cell membranes both contain a high level of PS [25], and this PS enrichment is promoted by Env-receptor interaction [26].

HIV entry into cells also requires cholesterol in both the host cell and the virion membranes [27]. Removal of cholesterol abrogates gp41-mediated liposome fusion [28], and cholesterol-depleting drugs such as statins inhibit HIV entry into macrophages [29]. Cholesterol affects influenza virus fusion in a more complicated manner [30]. Increasing the cholesterol content in target cell membranes accelerates lipid and content mixing. In contrast, moderate reduction of the cholesterol level from the virus envelope facilitates fusion while complete depletion of cholesterol slows fusion. This multiphasic effect was interpreted as resulting from the lateral organization of the membrane and cholesterol's effect on the mechanical properties of the membrane.

To better understand the mechanisms of protein-mediated membrane fusion, many biophysical studies have employed synthetic lipid mixtures that contain 5–6 components to mimic the HIV-1 envelope composition [14,18,28,31]. Derived from the host cell plasma membranes, the HIV envelope contains phosphocholine (PC), phosphoethanolamine (PE), phosphoserine (PS), sphingomyelin (SM), and cholesterol. The percentages of these lipids are somewhat different from those of the host cell plasma membrane (Table 1) [32,33]. The PC content is ~16% of all lipids in MT-4 plasma membranes but decreases by half (to ~8%) in the virion envelope. In comparison, PS and sphingolipid contents increase from the plasma membrane to the HIV-1 virion, while PE and plasmalogen (pl) PE lipids have counter-directional percentage changes. Cholesterol is enriched in the HIV envelope and is estimated to range from 32% to as much as 45% [32,33]. For each HIV-1 virion, about 160,000 phospholipids and sphingolipids and about 130,000 cholesterol molecules [32] together solvate 10–19 Env trimers [34].

An implicit assumption in using complex lipid mixtures for studying membrane fusion is that the lipids are homogeneously distributed in the membrane to induce the biologically relevant protein structure and function. However, the average lipid composition of the whole membrane does not necessarily reflect which lipids are abundant at the fusion

Table 1
The lipid mole percentages in MT-4 plasma membranes and MT-4 derived HIV virions. Adapted from quantitative mass spectrometry data of Lorizate and coworkers [33].

Lipids	MT-4 plasma membrane	MT-4 derived HIV
Cholesterol	32.4%	32.7%
Sphingolipids	13.9%	16.0%
PC	15.5%	7.9%
PE	9.7%	5.6%
pl-PE	12.3%	20.9%
PS	11.6%	15.2%
PI	4.4%	1.0%
PG	0.1%	0.7%
Total	100%	100%

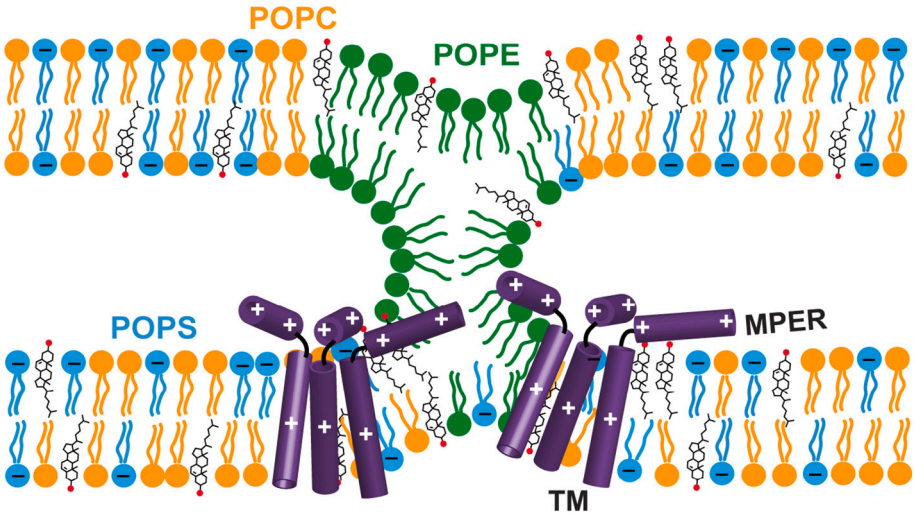

Fig. 1. Schematic model of the possible effects of gp41 MPER-TMD trimers on membrane structure and dynamics, to be investigated by the experiments shown in this work. The peptide might coordinate with negative-curvature lipids such as POPE (green) to induce negative Gaussian curvature. The peptide might change lipid mobility and membrane surface hydration to charged lipids such as POPS (blue) and zwitterionic lipids such as POPC (orange). At neutral pH, MPER-TMD contains +3 charges. Two MPER-TMD trimers are depicted schematically, but the data here do not probe whether multiple trimers are in close proximity.

site. For example, cholesterol is known to be inhomogeneously distributed in biological membranes [35]. If both host cell and HIV membranes have an inhomogeneous distribution of lipids, one can obtain more mechanistic insights by studying gp41 interactions with specific lipids, which may be enriched near the gp41 trimers. Therefore, to understand the protein-lipid interplay that causes membrane fusion, simplified 2- or 3-component model membranes are useful.

Here we present a ^{31}P solid-state NMR study of the structural and dynamical response of POPE, POPC, POPS and cholesterol to the gp41 MPER-TMD peptide. Specifically, we investigate membrane curvature, membrane surface hydration, and lipid dynamics in the presence of MPER-TMD (Fig. 1). MPER-TMD is an independent fusion-competent domain [14], and contains the epitopes for several broadly neutralizing antibodies (bnAbs) of HIV-1. We use static ^{31}P solid-state NMR lineshapes to detect nonlamellar membrane morphologies, direct-polarization (DP) and cross-polarization (CP) ^{31}P spectral intensities to probe lipid dynamics, and 2D ^{1}H-^{31}P correlation spectra to detect membrane hydration. These studies are conducted in one- to three-component lipid mixtures in order to assess the effects of gp41 on individual lipids. For some of the lipid mixtures, we varied the peptide-lipid molar ratio and lipid-cholesterol (CHOL) molar ratio to examine how the formation of nonlamellar phases depends on the lipid concentration. Our data show that POPE is the main lipid that generates NGC in the presence of gp41, that cholesterol inhibits this curvature effect, and that all phospholipids (PE, PS and PC) are more mobile and *better* hydrated in the presence of the peptide. These results give new and, in some cases, unexpected insights into the interplay between gp41 and lipids to cause membrane restructuring for virus-cell fusion.

2. Materials and methods

2.1. Peptide synthesis

The MPER-TMD peptide used in this work corresponds to residues 665–704 of gp41 (KWASLW NWFNITNWLW YIKLFIMIVG GLVGLRIVFA VLSI) from HIV-1 clade B, HXB2 isolate (UniProtKB/Swiss-Prot: P04578.2) [36]. The peptide was synthesized using Fmoc solid-phase chemistry on a custom designed flow peptide synthesizer [37]. It was synthesized on the 0.05 mmol scale using H-Rink amide ChemMatrix resin (0.1 g at 0.5 mmol/g loading size). The resin was swelled in the reaction vessel for 5 min in ~5 mL of *N*, *N*-dimethylformamide (DMF) at 70 °C. A 20-fold excess (1 mmol) of unlabeled amino acid was singly coupled with a coupling time of 50 s. After the final coupling step, the peptide was deprotected and cleaved from the resin by addition of TFA: phenol:H_2O:TIPS solution (88:5:5:2 by volume) for 3 h. The resin was filtered off, and the crude peptide was precipitated and triturated three times with cold diethyl ether and dissolved in 80% HFIP (1,1,1,3,3,3-hexafluoro-2-propanol) solution. Crude peptide was purified by reverse-phase HPLC using a Vydac C4 column with a linear gradient of 20–99% channel A over 120 min at a flow rate of 15 mL/min (where channel A is 1:1 v/v acetonitrile:isopropanol and channel B is acetonitrile). MALDI-MS analysis verified the mass to be 4781.5 Da, in good agreement with the calculated mass of 4781.8 Da. The peptide synthesis and purification yield was ~14%. The purity of the peptide was >95% based on HPLC and MS data.

2.2. Preparation of proteoliposomes

Three phospholipids were used in this study: 1-palmitoyl-2-oleoyl-sn-glycero-3-phosphoethanolamine (POPE), 1-palmitoyl-2-oleoyl-sn-glycero-3-phosphocholine (POPC), and POPC: 1-palmitoyl-2-oleoyl-sn-glycero-3-phospho-L-serine (POPS) (7:3). We chose POPX (X = C, E, S) lipids over saturated lipids such as DMPC in order to better mimic the acyl chain compositions of biological membranes. These lipids were mixed with cholesterol (CHOL) and with each other to produce several membrane mixtures: POPE, POPE:CHOL, POPC, POPC:CHOL, POPC: POPS (7:3), and POPC:POPS:CHOL (7:3:2). The CHOL concentrations in these membranes ranged from 0 to 17 mol% of total phospholipids, while the peptide monomer:phospholipid molar ratio (P/L) ranged from 0 to 1:10. A typical sample contained ~1 mg peptide, 5–16 mg of lipids and cholesterol, and 4–10 mg of water to reach ~40% hydration by mass.

For each membrane sample, the appropriate mass of MPER-TMD was dissolved in ~500 μL TFE. Phospholipids and cholesterol were each dissolved in 200–500 μL chloroform. A drop of methanol was added when needed to fully dissolve POPE. The resulting homogeneous lipid solution was added to the peptide TFE solution. The lipid vial was rinsed with another ~200 μL chloroform, combined with the protein-lipid solution, then transferred to a 20-mL scintillation vial and incubated for 10 min at room temperature. The chloroform and TFE were then removed under nitrogen gas for 15–60 min, and the vial was covered with a Kimwipe and placed in a vacuum chamber for 30–60 min to remove residual solvent.

Proteoliposomes were prepared by resuspending the 5–16 mg peptide-lipid mixture in 2 mL buffer (10 mM pH 7.4 HEPES/NaOH buffer, 1 mM EDTA, and 0.1 mM NaN_3), then homogenizing the vesicle solution by one of two methods. For POPC:POPS mixtures, we conducted 10–15 cycles of freeze-thaw between liquid nitrogen and 50 °C. For POPE-containing membranes, which do not homogenize well by the freeze-thawing method, we sonicated the vesicle solution at room temperature using a bath sonicator for at least three rounds of seven minutes each until the solution appeared homogeneous. The proteoliposome solutions were ultracentrifuged in a Beckman Coulter Optima LE-80 K centrifuge using a SW-60 swinging bucket rotor at a speed of 40,000–45,000 rpm (143,000–272,000 ×*g*) at 4 °C for 4–5 h. The wet membrane pellet was slowly dried to a hydration level of 35–50% (w/w) in a desiccator, then spun into a 4 mm MAS rotor through a 5 mL pipette tip in a Thermo Sorvall ST 16R centrifuge.

2.3. Solid-state NMR experiments

All static and MAS NMR experiments were conducted on a Bruker 400 MHz (^{1}H Larmor frequency) wide-bore AVANCE III-HD spectrometer using a 4 mm MAS probe tuned to ^{1}H/^{31}P frequencies. For static 1D ^{31}P experiments, the number of scans varied between 1024 and 20,480 to obtain sufficient signal-to-noise ratios for membrane samples of different masses. Unless otherwise noted, ^{31}P NMR experiments were conducted at a set temperature of 298 K for static experiments and 293 K for MAS experiments. Typical radiofrequency (RF) field strengths were 30–50 kHz for ^{1}H and 50 kHz for ^{31}P. The ^{31}P chemical shifts were referenced to the hydroxyapatite signal at 2.73 ppm on the phosphoric acid scale. 1D ^{31}P MAS cross-polarization (CP) and direct-polarization (DP) experiments used a ^{31}P RF field strength of 50 kHz, 3 ms CP at a ^{1}H RF field of 50 kHz, and a ^{1}H decoupling field of 40–50 kHz, for 1024 scans. ^{1}H chemical shifts were referenced to the lipid chain-end ω signal at 0.9 ppm. All MAS experiments were conducted under 5 kHz MAS. At this spinning frequency, a set temperature of 290–300 K gives sample temperatures that are at most 5 °C higher than the thermocouple reported temperature. The sample temperature is estimated from the water ^{1}H chemical shifts measured on a POPC sample containing a small amount of DSS, and is consistent with the reported minimal heating at this MAS rate [38]. Water ^{1}H T_1 relaxation times were measured using the inversion recovery experiment with variable delays (τ) of 0.01, 0.05, 0.1, 0.25, 0.5, 0.75, 1, 1.75, 2.5, 3.25, and 4.0 s. Most samples contained two populations of water, corresponding to tightly bound versus loosely membrane-associated water [39]. Thus, we fit the inversion recovery intensities using a bi-exponential function $I(\tau) = A(1 - 2e^{-\tau/T_{1a}}) + (1 - A)(1 - 2e^{-\tau/T_{1b}})$. The population factor A was at least 0.9 in each sample, so we used the larger T_1 value, which represents bulk water, to correct for the ^{1}H spin diffusion buildup intensities.

To measure the water accessibility of phospholipids, we conducted a 2D ^{1}H-^{31}P heteronuclear correlation (HETCOR) experiment with ^{1}H spin

diffusion. The pulse sequence starts with four ^{31}P 90° pulses spaced by 2 ms each to saturate the ^{31}P magnetization, then a ^{1}H 90° excitation pulse and a ^{1}H T_2 filter (2 * 0.745 ms = 1.49 ms) to select for the water and lipid ^{1}H magnetization. The 2D experiments used 150 t_1 time points to reach a maximum evolution time of 15 ms, and 64–128 scans per t_1 increment. The ^{1}H chemical shift evolution period was followed by a variable mixing time τ_m, during which the water and lipid chain ^{1}H magnetization is transferred to lipid headgroup and glycerol protons, then detected on ^{31}P following CP. The ^{1}H-^{31}P HETCOR spectra were measured with ^{1}H spin diffusion mixing times of 4 to 900 ms to extract the spin diffusion buildup curves. The 2D HETCOR spectra for comparing water-^{31}P cross peak intensities were measured using 25 ms mixing for the POPC/POPS samples and 64 ms for the POPE samples.

All NMR spectra were plotted from TopSpin 3.6.1. For each static ^{31}P spectrum that exhibits a strong isotropic peak, we matched the 90°-edge intensities of the peptide-free control spectrum and the peptide-containing spectrum, then subtracted the control spectrum to obtain a difference spectrum that exhibits only the isotropic peak. The difference spectrum was integrated over the chemical shift range of the isotropic peak while the peptide-containing spectrum was integrated over the entire spectral range. The ratio of these integrated intensities represents the percentage of the isotropic peak in the peptide-containing spectrum.

To obtain spin diffusion buildup curves, we divided the water-POPS cross peak intensities as a function of τ_m by $e^{-\tau_m/T_1}$, using the aforementioned bulk-water ^{1}H T_1 values, to correct for spin-lattice relaxation of water [40]. The T_1-corrected intensities were then normalized to the 900 ms value. Error bars reflect the propagated signal-to-noise ratios of the water-^{31}P cross peaks. The ^{31}P chemical shift anisotropy (CSA) values ($\Delta\sigma$) were read off as the difference between the downfield 0° edge (σ_{11}) of the powder pattern and the upfield 90° edge (σ_{33}).

3. Results

We first investigated gp41-induced membrane curvature using static ^{31}P NMR spectra. We compared POPE, POPC and POPC:POPS membranes with and without cholesterol and as a function of P/L ratio. POPE has intrinsic negative curvature, which makes POPE-containing membranes prone to develop NGC in the presence of various membrane-active peptides such as antimicrobial peptides [20,41,42] and influenza M2 [21]. POPC is abundant in eukaryotic membranes [43], whereas the negatively charged POPS has been implicated as a cofactor for HIV entry into macrophages [25]. The POPC:POPS (7:3) membrane is therefore useful for investigating the effect of negative membrane surface charge on fusion.

3.1. MPER-TMD changes the POPE membrane curvature in a cholesterol-dependent manner

Fig. 2 shows the static ^{31}P NMR spectra of POPE membranes with varying concentrations of cholesterol and peptide. The ^{31}P spectra were measured at 298 K and 310 K to compare the membrane curvature near and well above the main phase transition temperature of POPE (25 °C). The peptide-free POPE membranes with and without cholesterol both show the expected uniaxial powder line shapes that are characteristic of a lamellar bilayer. Table 2 shows the ^{31}P CSA and the isotropic intensity fractions. Given the sensitivity of the high-temperature spectra to membrane defects, and the physiological relevance of 310 K for examining virus-cell fusion, we focus our spectral comparison on the 310 K data. At 310 K, the ^{31}P CSA of pure POPE membrane is 43.4 ppm, consistent with a liquid-crystalline membrane. Addition of the peptide at a P/L of 1:100 causes a small isotropic peak. This isotropic peak is reversible: cooling the membrane down to lower temperature suppressed the isotropic peak (data not shown), indicating that the isotropic peak results from a high-curvature membrane phase rather than formation of permanent morphologies such as membrane buds. Further increasing the peptide concentration to P/L = 1:20 dramatically changed the POPE spectra, causing a prominent isotropic peak that represents ~75% of the total spectral intensity. However, at 298 K this isotropic peak percentage decreases to ~15%. We attribute this large change in the isotropic peak intensities to faster lipid lateral diffusion at 310 K over the surface of the membrane, which should better sample the curvature of the POPE membrane.

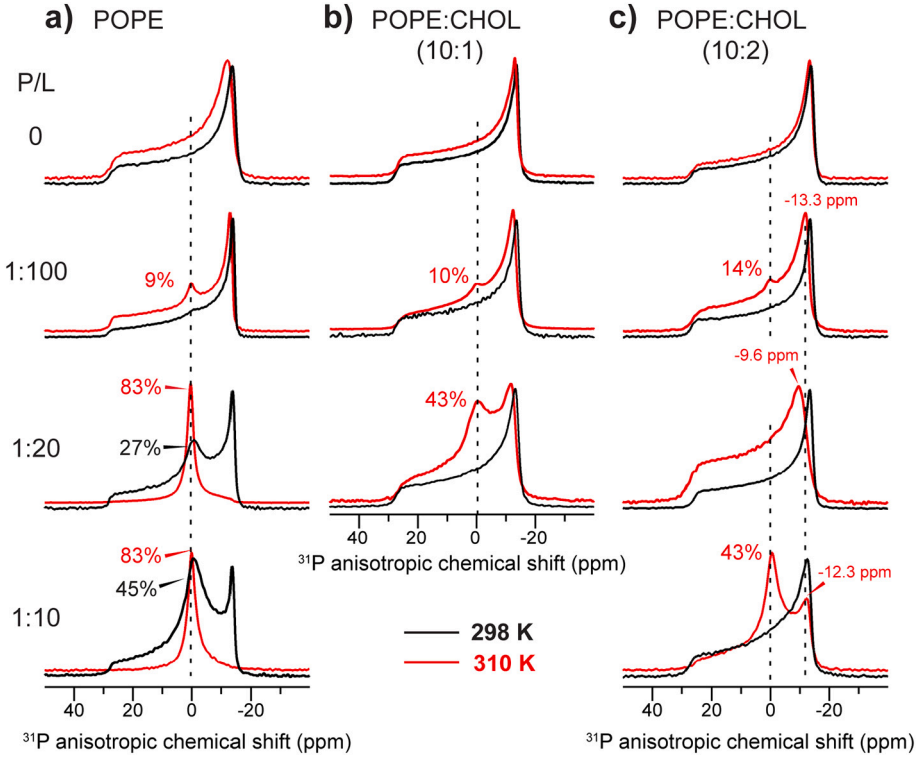

Fig. 2. Static ^{31}P NMR spectra of POPE membranes with varying cholesterol and peptide concentrations. The P/L ratio increases from top to bottom (0 to 1:10), while the cholesterol concentration increases from left to right. Spectra were measured at 298 K (black) and 310 K (red). (**a**) ^{31}P spectra of CHOL-free POPE membranes. (**b**) ^{31}P spectra of POPE:CHOL (10:1) membranes. (**c**) ^{31}P spectra of POPE:CHOL (10:2) membranes. Dashed lines guide the eye to the POPE isotropic chemical shift. The approximate intensity fraction of the isotropic peak relative to the full spectrum is indicated for various spectra.

Table 2
^{31}P chemical shift anisotropies ($\Delta\sigma = \delta_{11} - \delta_{33}$ by the Herzfeld-Berger convention) and percentages of the isotropic component, in the static ^{31}P NMR spectra of lipid membranes with different P/L ratios and at two set temperatures.

Membrane	P:L	298 K		310 K	
		Isotropic %	Δσ (ppm)	Isotropic %	Δσ (ppm)
POPE	0	0%	44.2	0%	43.4
	1:100	0%	43.5	9%	44.0
	1:20	27%	42.7	83%	44.4
	1:10	45%	43.3	83%	–
POPE:Chol (10:1)	0	0%	43.7	0%	43.0
	1:100	0%	42.3	10%	41.4
	1:20	0%	42.2	43%	41.2
POPE:Chol (10:2)	0	0%	43.6	0%	40.2
	1:100	0%	42.7	14%	41.6
	1:20	0%	41.2	0%	40.0
	1:10	0%	42.1	43%	39.3
POPC	1:100	0%	46.7	0%	45.2
	1:10	0%	45.1	0%	45.2
POPC:CHOL (10:2)	1:100	0%	46.9	0%	45.4
	1:10	0%	45.8	0%	45.2
POPC:POPS (7:3)	1:100	0%	55.2, 44.1	0%	53.9, 42.6
	1:40	0%	51.7, 42.9	0%	52.7, 40.5
POPC:POPS:CHOL (7:3:2)	1:100	0%	53.5, 44.0	0%	53.1, 42.6
	1:40	0%	52.1, 42.0	0%	51.9, 40.7

Increasing the cholesterol concentrations in the POPE membrane reduced the isotropic ^{31}P intensity. In membranes containing 17% cholesterol, the isotropic peak is undetectable at P/L = 1:20. However, as the peptide concentration increased to P/L = 1:10, the isotropic peak increased to 64% even in the presence of 17% cholesterol. Moreover, the combination of peptide and cholesterol narrowed the ^{31}P CSA from 43 to 44 ppm down to 39–42 ppm by the Herzfeld-Berger convention (see Table 2).

For long-chain phospholipids such as POPE and DOPE, the isotropic peak in the static ^{31}P spectra do not result from isotropic micelles but correspond to bicontinuous lipid cubic phases [24]. This has been shown by ^{31}P T_2 relaxation times and SAXS data [22]. These lipid cubic phases possess NGC on every point of the membrane surface. Due to their cubic symmetry, lipid lateral diffusion over these bicontinuous phases averages the ^{31}P chemical shift to its isotropic value. Since this translational diffusion occurs over tens of nanometers of the cubic phase dimension, the reorientational rate is slower than the local uniaxial diffusion rate of lipids or the tumbling of detergent micelles in solution. Therefore, the isotropic peak of cubic-phase lipids is usually much broader than the isotropic peak of micelles, and the ^{31}P T_2 relaxation times of cubic phase lipids are also much shorter than those of micelles. The isotropic peaks seen in our static ^{31}P spectra are relatively broad, which is consistent with the cubic-phase interpretation. In principle, these isotropic peaks could also reflect membrane buds. But given the non-spontaneous nature of membrane budding, this interpretation is less likely. Further experiments are needed to distinguish these possibilities. The increasing isotropic peak intensity of the POPE membranes with increasing peptide concentration indicates that the NGC curvature induction is directly caused by gp41 MPER-TMD.

Interestingly, for the POPE:CHOL (10:2) membrane at 310 K, cholesterols inhibitory effect on peptide-induced membrane curvature is not monotonic with the peptide concentration (Fig. 2c). The isotropic peak is small at P/L = 1:100, undetectable at 1:20, and dominant at P/L = 1:10. This non-monotonic dependence on peptide concentration was reproducible. However, the 1:20 spectrum has a narrower ^{31}P CSA than the 1:100 and 1:10 spectra, manifested by the fact that the maximum of the powder pattern is shifted downfield by 2.4 ppm compared to the 1:100 spectrum. This observation suggests that the POPE lateral diffusion may be faster at 1:20 than at lower or higher P/L ratios, thus obscuring the isotropic peak.

3.2. MPER-TMD does not cause curvature to POPC and POPC:POPS membranes

To investigate whether MPER-TMD not only causes curvature to POPE membranes but also to lipid membranes without spontaneous negative curvature, we measured the ^{31}P static spectra of POPC and POPC:POPS (7:3) membranes without and with cholesterol (Fig. 3). Fig. 3a, b shows that the gp41 peptide caused little nonlamellar morphology to POPC and POPC:CHOL membranes. Even at a high P/L of 1:10, only a small isotropic peak representing less than 7% of the spectral intensity is observed. Similarly, the POPC:POPS membranes showed little isotropic intensity, although at P/L = 1:40 a small isotropic peak is detected (Fig. 3c). This peak was removed by the addition of cholesterol (Fig. 3d).

The use of POPS also allows us to investigate the effects of negative membrane surface charge on curvature generation. The ^{31}P spectra of POPC:POPS samples with 1:100 peptide reveal two powder patterns, with maximum intensities at −14.6 ppm and −18.1 ppm at 298 K (Fig. 3c; Table 2). Based on the pure POPC spectra, we tentatively assign the smaller CSA to POPC and the larger CSA to POPS. In principle, the different CSAs could result from POPC and POPS phase separation into microdomains, as found in solid-supported POPC:POPS (4:1) bilayers in the presence of 1 mM calcium ions based on scanning force microscopy data [44]. However, differential scanning calorimetry data showed that, in the absence of calcium, PC and PS with similar acyl chains and at PS concentrations of 30 mol% do not phase separate above the phase

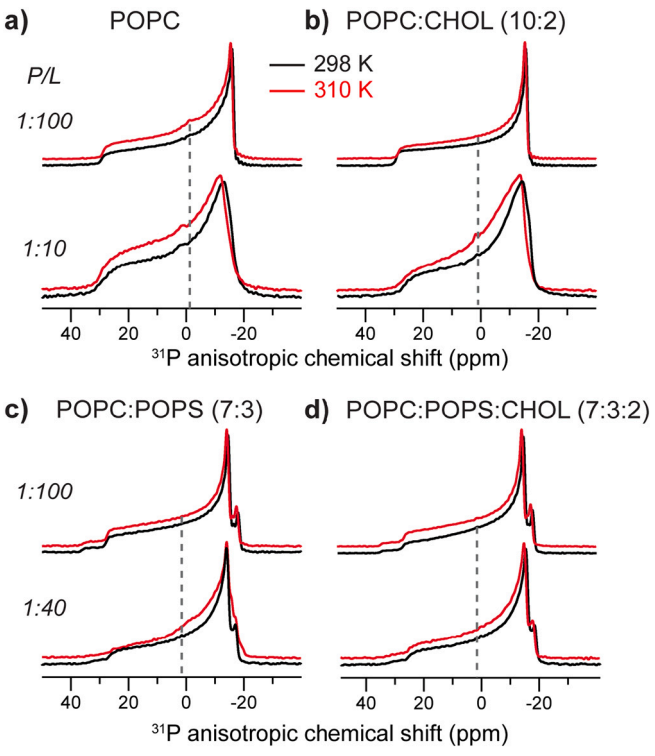

Fig. 3. Static ^{31}P NMR spectra of POPC and POPC:POPS membranes with varying MPER-TMD and cholesterol concentrations. (**a**) POPC membrane. (**b**) POPC:CHOL (10:2) membrane. (**c**) POPC:POPS (7:3) membrane. (**d**) POPC:POPS:CHOL (7:3:2) membrane. The P/L molar ratios are 1:100, 1:40, or 1:10, as shown on the left of each spectrum. ^{31}P spectra were measured at 298 K (black lines) and 310 K (red lines). Dashed lines guide the eye to the isotropic chemical shift.

transition temperature of the individual lipids [45]. Thus, the different ^{31}P CSAs more likely reflect distinct headgroup orientations and conformations of POPC and POPS [46]. Addition of the peptide broadened the linewidths and obscured the two 90° edges, indicating that the peptide changed the lipid mobilities (*vide infra*).

3.3. MPER-TMD increases the mobility of all phospholipids

In addition to membrane curvature, two other features of membrane fusion that have been postulated are increased lipid mobilities and dehydration of the membrane surface in fusion intermediates [47]. The increased lipid mobilities were proposed to result from the membrane curvature at the site of fusion and the disordering effect of the fusion protein. The dehydration barrier against two opposing lipid bilayers results from charge repulsion between polarized water molecules on the two membrane surfaces [5,6,48]. To investigate the effects of MPER-TMD on lipid dynamics, we measured ^{31}P DP and CP MAS spectra. The ^{31}P DP spectral intensities reflect the amounts of phospholipids in the sample, while the CP intensities are reduced for dynamic molecules due to motional averaging of the ^{1}H-^{31}P dipolar coupling. Therefore, a lower intensity ratio of CP to DP spectra indicates a higher mobility of phospholipids [49,50].

Fig. 4 compares the DP- and CP-MAS spectra of POPE and POPC:POPS membranes without and with MPER-TMD and with and without cholesterol. For the POPE membrane, addition of the peptide reduced the CP/DP intensity ratios at 310 K (Fig. 4a) and 293 K (data not shown), indicating that MPER-TMD increased the POPE mobility. When cholesterol is present, this intensity change is abolished (Fig. 4b): the peptide-containing sample exhibits the same CP/DP intensity ratio as the peptide-free membrane, indicating that cholesterol abrogates the peptide's ability to increase the POPE mobility. For POPC:POPS and POPC:POPS:CHOL membranes (Fig. 4c, d), the peptide lowered the CP intensities relative to the DP intensities, indicating that the peptide increased the dynamics of both POPC and POPS. However, the POPS CP intensities decreased more than those of POPC (Fig. 4e), indicating that POPS is disordered by gp41 more than POPC is. This observation is consistent with the preferential line broadening of the POPS signal in the static ^{31}P NMR spectra (Fig. 3c) and MAS DP spectra (Fig. 4d).

3.4. MPER-TMD increases membrane surface hydration

To investigate membrane surface hydration, we measured 2D ^{1}H-^{31}P correlation spectra with ^{1}H spin diffusion under MAS [51]. This experiment selects the dynamic water and lipid ^{1}H magnetization with a ^{1}H T_2 filter, then transfers the magnetization to ^{31}P for detection. The water ^{1}H polarization transfer is mediated by chemical exchange and spin diffusion. For proteoliposome mixtures with exchangeable protons in the lipid headgroup or near the membrane surface, the water-^{31}P cross peak

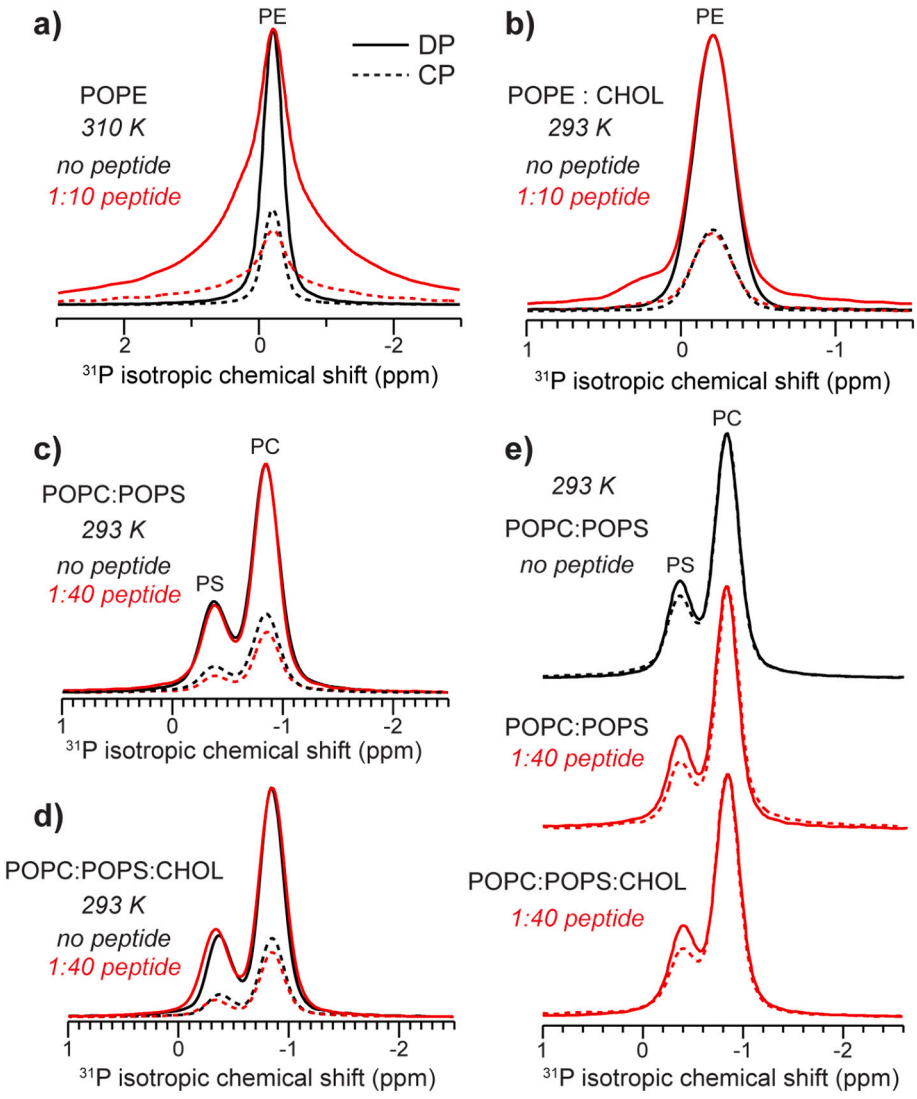

Fig. 4. ^{31}P CP-MAS (dashed lines) and DP-MAS (solid lines) spectra showing the effects of the gp41 MPER-TMD on phospholipid dynamics. The samples were spun at 5 kHz. Peptide-free spectra are shown in black while peptide-containing spectra are shown in red. For each panel, the peptide-free and peptide-containing DP spectra are scaled to match the intensities, so that the different intensities of the CP spectra indicate the different CP efficiencies of the two samples. (**a**) POPE spectra measured at 310 K. MPER-TMD decreased the CP intensities relative to the DP intensities, indicating that the peptide increased POPE dynamics. (**b**) POPE:CHOL (10:2) spectra measured at 293 K. (**c**) POPC:POPS (7:3) spectra without and with the peptide. The peptide decreased the CP intensities of both POPC and POPS relative to the DP intensities, indicating that it increased lipid dynamics. (**d**) POPC:POPS:CHOL (7:3:2) spectra. The gp41 peptide decreased the CP efficiency as in (**c**). (**e**) DP and CP spectra of three POPC:POPS membranes: POPC:POPS (7:3) without the peptide, POPC:POPS (7:3) membrane with 1:40 peptide, and POPC:POPS:CHOL (7:3:2) with 1:40 peptide. When each pair of spectra are scaled to match the DP and CP intensities of the POPC peak at around −0.84 ppm, the POPS CP intensity decreases relative to the DP intensity, indicating that POPS mobility is preferentially enhanced compared to that of POPC by the peptide.

intensity reflects the water accessibility and water dynamics of the membrane surface. Lipid protons also correlate with ^{31}P after spin diffusion [51], and the lipid ^{1}H chemical shifts can be readily assigned based on literature values [52,53].

Fig. 5 shows the 2D HETCOR spectra of the POPE and POPE:CHOL (10:2) membranes in the absence and presence of MPER-TMD. With 64 ms ^{1}H mixing, all protons of the lipid headgroup, glycerol backbone, and acyl chains down to the chain-end ω, are detected. The highest cross peak intensities are observed for the headgroup Hα and the glycerol backbone G3, as expected due to their spatial proximity to the phosphate group. No water cross peak is observed for the POPE membranes either with or without the peptide (Fig. 5a). This is consistent with the generally low hydration of the POPE membrane surface, as also seen, for example, for POPE membranes containing the PIV5 fusion protein's transmembrane domain [22]. The addition of cholesterol changed the situation: while the peptide-free POPE:CHOL membrane still showed no cross peak, the peptide-bound sample exhibits a clear water cross peak (Fig. 5b), indicating increased hydration when both cholesterol and the peptide are present in the membrane. The water peak has a relatively broad linewidth of ~0.3 ppm, which may be attributed to chemical exchange of bound water with the POPE amino group and the low mobility of membrane surface water for the hydrogen-bonded POPE headgroups.

We investigated the hydration of POPC using the same 2D ^{1}H-^{31}P correlation experiment (Fig. 6). Although the POPC headgroup itself has no exchangeable protons, with a long ^{1}H mixing time of 225 ms and due to relayed polarization transfer through POPS, cholesterol and the peptide, we can still detect water-^{31}P cross peaks [51]. Fig. 6a–c show that in POPC:POPS membranes with and without cholesterol, the peptide dramatically increased the intensity of the water cross peak to POPC. Similarly, for POPC membranes with and without cholesterol, the addition of MPER-TMD caused a water-^{31}P cross peak, whereas no water cross peak is detected in the absence of the peptide (Fig. 6d–f). Water to POPC magnetization transfer can occur as a result of increased membrane surface hydration by the peptide and/or increased number of labile protons provided by the peptide. However, other viral fusion proteins' hydrophobic domains have been reported to show little water polarization transfer to POPC [54] (*vide infra*), suggesting that the higher water cross peak detected here likely reflects a true increase of POPC hydration by MPER-TMD.

Fig. 7 shows the 2D ^{1}H-^{31}P correlation spectra of POPC:POPS membranes measured with a shorter ^{1}H spin diffusion mixing time of 25 ms to study POPS hydration. The addition of MPER-TMD clearly increased the water-POPS cross peak intensities in the CHOL-free POPC:POPS membrane (Fig. 7a, b). The presence of cholesterol dampened this hydrating effect by the peptide (Fig. 7c, d). To quantify the cross peak intensity changes, we measured the 2D spectra as a function of the ^{1}H mixing time (Fig. 8). In the cholesterol-free POPC:POPS membrane, the water-POPS cross peak intensity buildup rate clearly increased with the peptide concentration (Fig. 8a), indicating that MPER-TMD facilitates POPS hydration in the mixed membrane. However, when cholesterol is present in the membrane, the peptide had a more modest hydration effect (Fig. 8b): the water-POPS buildup rates increased with peptide concentration to a smaller extent than in the cholesterol-free membrane.

4. Discussion

The ^{31}P NMR data shown above describe several different effects of gp41 MPER-TMD on membrane structure and dynamics. First, static ^{31}P NMR line shapes indicate that POPE is the most conducive phospholipid to NGC formation, while cholesterol counters this curvature induction (Figs. 2, 3). The pronounced NGC of the peptide-containing POPE membrane is consistent with the intrinsic negative curvature of POPE [55], which can promote NGC in concert with the positive membrane curvature created by the surface-bound MPER. In comparison, cholesterol, which also exhibits moderate negative curvature, weakens the nonlamellar morphology, as shown by the attenuated isotropic ^{31}P peak (Fig. 2). This effect suggests that the lipid shape is not the only determinant of NGC formation. We propose that a second factor for POPE-induced NGC is the hydrogen bonding of PE headgroups with each other, which dehydrates the membrane even in the absence of peptides, as seen in 2D ^{1}H-^{31}P correlation spectra (Fig. 5a).

Our approach deviates from those that replicate the *overall* lipid composition of the HIV membrane. When POPE is mixed with other lipids, including POPC, POPS, SM, and cholesterol, previous ^{31}P NMR spectra showed that the isotropic ^{31}P peak is largely removed [14,18,56]. Thus, dilution of the negative-curvature POPE by bilayer-stabilizing lipids attenuates membrane-curvature generation by gp41. The local lipid composition at the site of virus-cell fusion might deviate from the average lipid composition of the plasma membrane and the virus envelope, and might also fluctuate because of the preferential partitioning of gp41 to the boundary of the L_d and L_o phases [28]. Thus, the two- or three-component membrane mixtures examined here give insights into the membrane curvature that would appear when gp41 is surrounded by one or two types of phospholipids.

The bilayer-stabilizing effect of cholesterol may result from the well-

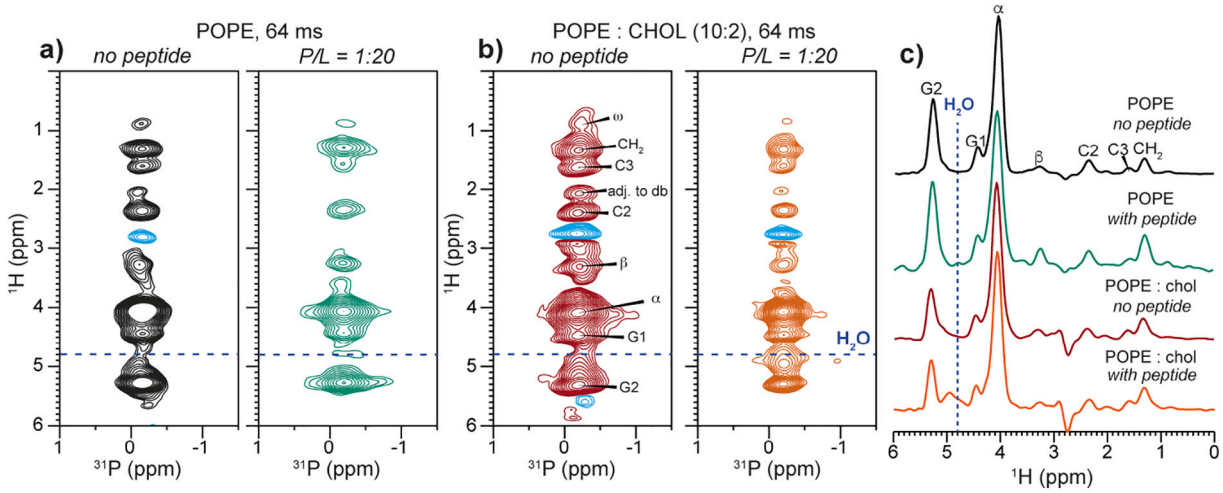

Fig. 5. 2D ^{1}H-^{31}P correlation spectra of POPE and POPE:CHOL (10:2) membranes without and with MPER-TMD, measured with a ^{1}H mixing time of 64 ms at 310 K. (**a**) POPE membranes without (black) and with (green) the peptide at a P/L of 1/20. (**b**) POPE:CHOL membranes without (red) and with (orange) the peptide at a P/L of 1:20. (**c**) ^{1}H cross sections of the four 2D spectra. The peptide caused a broad water peak only in the membrane containing both the peptide and cholesterol.

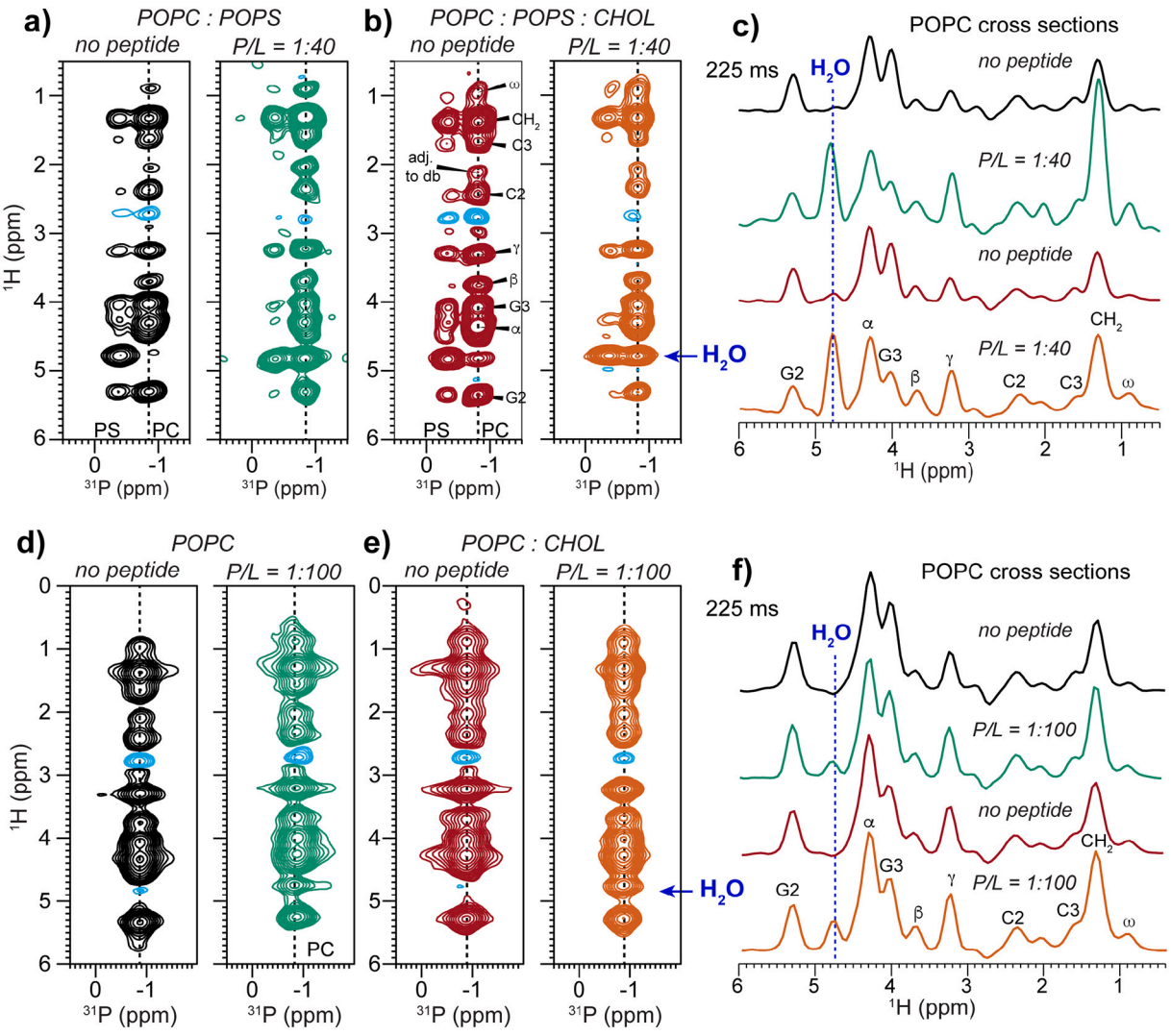

Fig. 6. 2D ^{1}H-^{31}P correlation spectra of POPC:POPS and POPC membranes without and with MPER-TMD. The spectra were measured with a ^{1}H mixing time of 225 ms at 293 K. (**a**) POPC:POPS (7:3) membranes without and with the peptide. (**b**) POPC:POPS:CHOL (7:3:2) membranes without and with the peptide. (**c**) POPC ^{1}H cross sections of the 2D spectra in (**a**) and (**b**), extracted from a ^{31}P chemical shift of −0.83 ppm (corresponding to POPC). Blue dashed lines guide the eye to the water ^{1}H chemical shift. The peptide-free membranes show no or weak water cross peaks while the peptide-containing samples show strong water cross peaks. (**d**) POPC membranes without and with peptide. (**e**) POPC:CHOL (10:2) membranes without and with peptide. (**f**) POPC ^{1}H cross sections of the 2D spectra in (d) and (e). The peptide moderately increases the water cross peak intensity.

known rigidification of the membrane by cholesterol at high temperature. With 17% cholesterol in the POPE membrane (Fig. 2c), we found that the percentage of nonlamellar morphologies is low except at the highest peptide concentration of P/L = 1:10. In POPC:POPS membranes containing 17% cholesterol, no isotropic peak is observed at P/L ratios up to 1:40 (Fig. 3d). These results indicate that cholesterol weakens the peptide-induced membrane curvature at concentrations above ~17%. Thus, the requirement of cholesterol for membrane fusion and HIV infection [27,28,57] might be due to mechanisms other than curvature generation. One mechanism might be regulation of lipid mixing. Cholesterol is known to alter the spatial distributions of lipids in a concentration-dependent manner. High cholesterol concentrations (40–50%) promote homogeneous mixing in normally phase-separated membranes such as DSPC:DPPC mixtures [58] and DOPC:DPPC:CHOL mixtures [59], whereas moderate cholesterol levels promote phase separation. For example, cholesterol creates PC-rich microdomains in polyunsaturated PC:PS:PE mixtures [60]. By separating lipids into multiple phases with different chain orders, cholesterol can increase the hydrophobic mismatch and hence the line tension at the L_d and L_o boundary, thus facilitating fusion. Indeed, total internal reflection fluorescence microscopy data showed that the gp41 FP is localized at the L_d-L_o boundary in phase-separated SM and PS membranes that contain 25% cholesterol [28] and line tension at those boundaries may contribute to fusion [61]. These biophysical data and our ^{31}P NMR results together indicate that the total cholesterol content in the membrane needs to be sufficiently high to support phase separation but not so high as to create a homogeneous membrane. At the same time, the *local* cholesterol concentration near gp41 needs to be moderate to allow curvature induction.

A second mechanism for the requirement of cholesterol for fusion might be the recruitment of gp41 by cholesterol into raft regions of the membrane. A recent solid-state NMR and molecular dynamics simulation study of cholesterol-gp41 interactions found that cholesterol is in molecular contact with the MPER in lipid membranes [56]. Moreover, cholesterol self-associates into dimers and higher-order oligomers in lipid bilayers [62]. Thus, cholesterol could serve to bring multiple gp41 trimers into close proximity (Fig. 1), facilitating virus-cell fusion. Finally, a biological mechanism by which cholesterol might mediate membrane fusion is that the cell-surface receptors recognized by Env reside in cholesterol-rich domains, so cholesterol depletion may inhibit

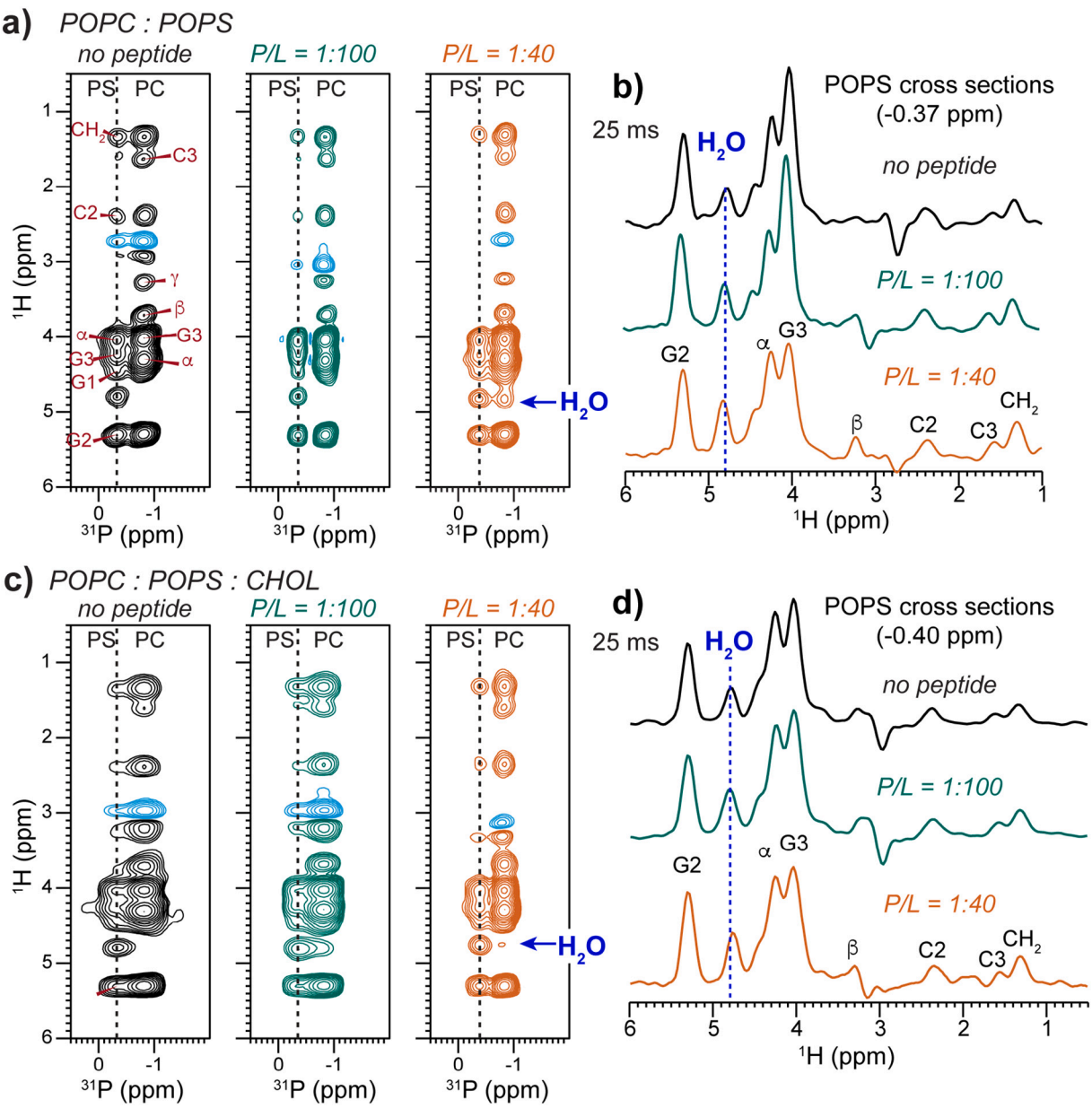

Fig. 7. 2D ^{1}H-^{31}P correlation spectra of POPC:POPS membranes without and with MPER-TMD and with and without cholesterol. The spectra were measured with a ^{1}H mixing time of 25 ms at 293 K. (**a**) 2D spectra of POPC:POPS membranes without the peptide, with P:L of 1:100 (green) and 1:40 (orange). (**b**) POPS ^{1}H cross sections of the POPC:POPS membranes for the three samples shown in (**a**). (**c**) 2D spectra of POPC:POPS:CHOL (7:3:2) membranes without the peptide, with P:L = 1:100 and 1:40. (**d**) POPS ^{1}H cross sections of the POPC:POPS:CHOL membranes. The peptide moderately increased the water cross peak with POPS.

gp120 binding to the receptors [29,63].

It is of interest to compare the curvature-inducing ability of gp41 MPER-TMD with that of other peptides involved in membrane fusion, such as gp41 FP and the PIV5 F protein's FP and TMD. ^{31}P NMR spectra of membranes containing these peptides indicate that MPER-TMD has weaker curvature-inducing ability than the HIV and PIV5 fusion peptides but similar curvature-inducing ability to the PIV5 TMD. The gp41 FP induced an isotropic peak to the static ^{31}P spectrum of an equimolar DOPC:DOPE:CHOL mixture, but did not induce an isotropic peak in the static spectrum of a virus-mimetic membrane (LM3) with less PE [31]. Thus, PE is synergistic with FP in causing membrane curvature. The gp41 FP induced an isotropic peak at a low P/L ratio of 1:50, indicating that it is more effective than the MPER-TMD in causing membrane curvature. The PIV5 FP generated high curvature to POPC membranes at a P/L of 1:15 [54] while MPER-TMD did not cause curvature to POPC membranes even at a higher P/L of 1:10. The influenza M2 protein, which has membrane scission activity, causes NGC in 30% cholesterol membranes at a P/L ratio of 1:15 [64]. In comparison, gp41 MPER-TMD has no such ability in the 33% cholesterol POPE membrane at a P/L ratio of 1:10, indicating that not all curvature-inducing peptides respond to cholesterol the same way. The PIV5 fusion protein TMD has a similar ability to gp41 MPER-TMD to cause curvature to PE membranes [22]. However, the PIV5 TMD does not possess a membrane-surface domain. Instead, its Val and Ile rich sequence adopts an unusual strand-helix-strand conformation, which was hypothesized to promote membrane curvature. Therefore, both the primary sequence and the three-dimensional structure impact membrane-curvature generation by these viral fusion protein hydrophobic domains.

The second conclusion from the current data is that gp41 MPER-TMD increases the dynamic disorder of multiple phospholipids, including PC, PE and PS. This is manifested by the lower CP intensities of the ^{31}P spectra relative to the DP spectra in the peptide-bound membranes,

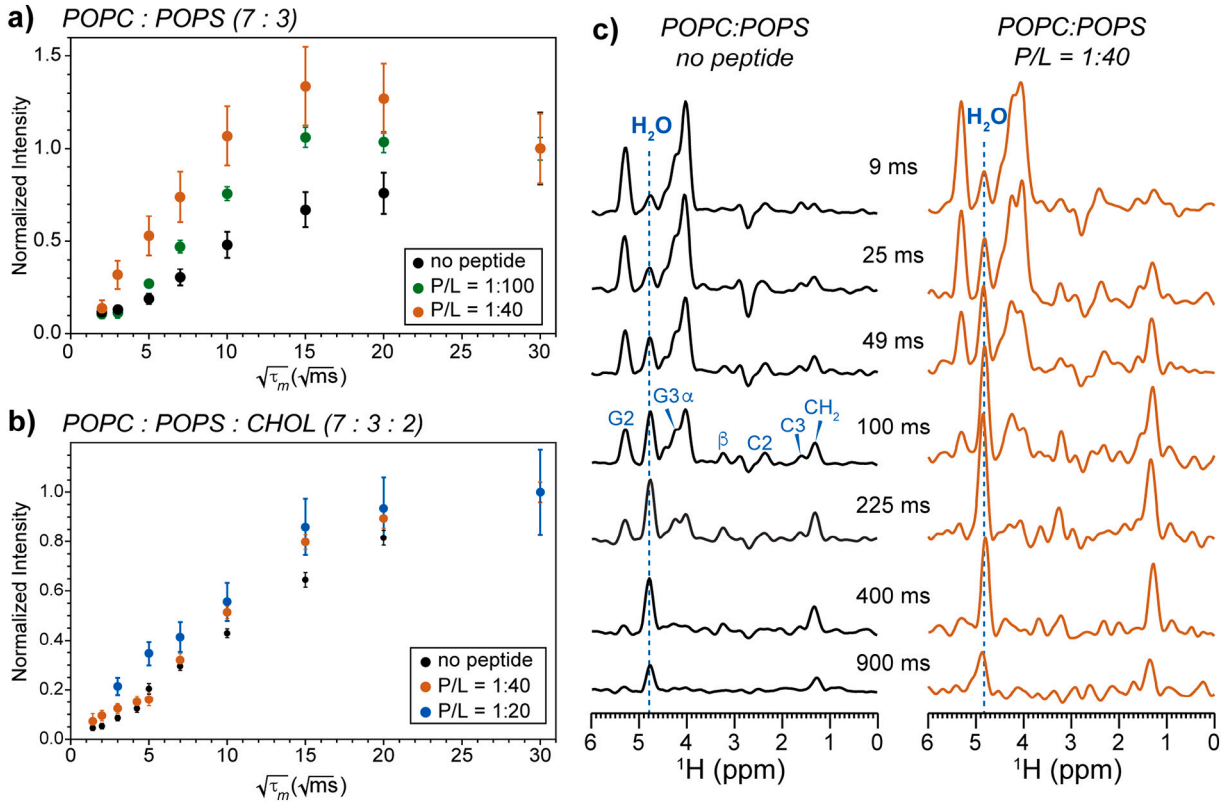

Fig. 8. Water ^{1}H magnetization transfer to POPS in POPC:POPS membranes containing varying concentrations of peptide and cholesterol. The buildup curves were extracted from 2D ^{1}H-^{31}P HETCOR spectra measured as a function of mixing time. (**a**) Water-POPS ^{1}H-^{31}P cross peak intensities in the POPC:POPS (7:3) membranes without the peptide (black), with 1:100 peptide (green), and 1:40 peptide (orange). Intensities have been corrected for water ^{1}H spin-lattice (T_1) relaxation. Error bars were propagated from the experimental signal-to-noise ratios. (**b**) Water-POPS cross peak intensities in POPC:POPS:CHOL (7:3:2) membranes without the peptide (black), with 1:40 peptide (orange), and with 1:20 peptide (blue). (**c**) POPS ^{1}H cross sections extracted from the 2D spectra of the POPC:POPS membrane (as in Fig. 7) without the peptide and with 1:40 peptide (data shown in panel a). Dashed blue lines guide the eye to the water ^{1}H chemical shift.

compared to peptide-free membranes (Fig. 4). The increased lipid mobility and disorder is expected for fusion intermediates. Since POPE resides in high-curvature membranes, we interpret the increased dynamic disorder as due to faster reorientation of POPE. In comparison, POPS exhibits the lowest CP intensities among the three phospholipids and its static linewidth also appears to be preferentially broadened by the peptide (Figs. 3c and 4d). These observations suggest that POPS may undergo slower, intermediate-timescale, motion in the presence of the peptide. This interpretation is consistent with a model where electrostatic attraction between negatively charged POPS headgroups and positively charged K665 and K683 in the MPER might slow POPS motion relative to POPC and POPE.

The third finding of the current data is that MPER-TMD increased, rather than decreased, the hydration of all phospholipids, irrespective of membrane curvature. This hydration effect is manifested by the higher water-^{31}P cross peaks in 2D ^{1}H-^{31}P correlation spectra (Figs. 5–7) and faster water to POPS ^{1}H magnetization transfer rates (Fig. 8). This enhanced water polarization transfer to lipids occurs *despite* the faster lipid motion. The POPE and POPS headgroups both contain exchangeable NH protons, thus water polarization transfer can proceed efficiently through chemical exchange and spin diffusion, regardless of the peptide. Both POPE and POPS showed higher cross peaks with water when the peptide is present, indicating increased hydration of the membrane surface. This increased hydration is opposite to the expectation for membrane fusion in the absence of proteins [48], where water expulsion is thought to be a necessary high-energy step. Instead, our data support a model wherein gp41 MPER-TMD reduces the dehydration energy barrier by coating the membrane surface with the MPER helices [14]. This potential alteration of the free energy of protein-free membrane fusion by reducing the dehydration barrier has also been proposed for other viral fusion proteins such as the PIV5 FP [65].

For gp41 MPER-TMD, another possible reason for the higher membrane hydration is the presence of a cationic arginine, R696, in the middle of the TMD (Fig. 1). Hydrogen-deuterium exchange NMR data show that the C-terminal TMD residues are more accessible to water than the N-terminal residues [66]. This water pathway in the trimeric helical bundle might increase the membrane's hydration. Interestingly, MD simulations of the gp41 TMD in DPPC and DPPC:CHOL membranes reported fluctuations of membrane thickness up to 7 Å, which correlate with a water defect near the Arg residue [67]. Moreover, this water defect is better localized in the cholesterol-containing membrane than in the cholesterol-free membrane. Thus, gp41 MPER-TMD might increase membrane hydration through the cationic R696.

The membrane-hydrating effect of gp41 MPER-TMD is the opposite of the effect of the PIV5 fusion protein on the membrane. Based on 2D ^{1}H-^{31}P correlation NMR spectra, we found that the PIV5 FP dehydrates POPC [54] and DOPE membranes [68] but hydrates the POPC:POPG membrane. This trend correlates with the secondary structure of the PIV5 FP: the more α-helical the peptide, the higher the membrane hydration. For the PIV5 fusion protein TMD, the peptide maintains the hydration of POPC and POPC:POPG membranes but dehydrates the POPE membrane, in which the TMD adopts the β-strand conformation [22]. Thus, for both the FP and TMD of the PIV5 fusion protein, the β-sheet conformation is correlated with membrane dehydration. In comparison, the α-helical gp41 MPER-TMD hydrates the membrane, and the gp41 chimera that covalently links the FP and MPER-TMD also increases membrane surface hydration [18]. Taken together, these data suggest that α-helical fusion protein domains maintain and even

increase the hydration of membrane surfaces. Only when β-strand conformations coat the membrane surface is dehydration observed.

In conclusion, the current ^{31}P solid-state NMR study shows that gp41 MPER-TMD relies on PE to induce the negative-Gaussian curvature that is required for hemifusion intermediates and fusion pores. This curvature-inducing action is accompanied by the peptide's ability to increase the dynamic disorder of the lipids, and by the attenuation of the dehydration barrier, both facilitating membrane merger. The observed bilayer-stabilizing effects of cholesterol suggest that cholesterol may not be enriched at the fusion site, which is consistent with biochemical finding that HIV-cell fusion occurs at the boundary between cholesterol-rich and cholesterol-poor regions of the membrane. Future elucidation of the molecular mechanism and pathway of Env-mediated HIV-cell membrane fusion should take into account the specific peptide-lipid interactions observed here.

Declaration of competing interest

The authors declare that they have no known competing financial interests or personal relationships that could have appeared to influence the work reported in this paper.

Acknowledgment

This work is supported by NIH grant GM066976 to M.H. This study made use of NMR spectrometers at the MIT-Harvard Center for Magnetic Resonance, which is supported by NIH grant P41 GM132079.

References

[1] D. Weissman, R.L. Rabin, J. Arthos, A. Rubbert, M. Dybul, R. Swofford, S. Venkatesan, J.M. Farber, A.S. Fauci, Macrophage-tropic HIV and SIV envelope proteins induce a signal through the CCR5 chemokine receptor, Nature 389 (1997) 981–985.
[2] B. Chen, Molecular mechanism of HIV-1 entry, Trends Microbiol. 27 (2019) 878–891.
[3] D.R. Burton, L. Hangartner, Broadly neutralizing antibodies to HIV and their role in vaccine design, Annu. Rev. Immunol. 34 (2016) 635–659.
[4] S.C. Harrison, Viral membrane fusion, Nature Struc. Mol. Biol. 15 (2008) 690–698.
[5] L.V. Chernomordik, M.M. Kozlov, Protein-lipid interplay in fusion and fission of biological membranes, Annu. Rev. Biochem. 72 (2003) 175–207.
[6] F.S. Cohen, G.B. Melikyan, The energetics of membrane fusion from binding, through hemifusion, pore formation, and pore enlargement, J. Membr. Biol. 199 (2004) 1–14.
[7] R.A. Lamb, T.S. Jardetzky, Structural basis of viral invasion: lessons from paramyxovirus F, Curr. Opin. Struct. Biol. 17 (2007) 427–436.
[8] H.S. Yin, X. Wen, R.G. Paterson, R.A. Lamb, T.S. Jardetzky, Structure of the parainfluenza virus 5 F protein in its metastable, prefusion conformation, Nature 439 (2006) 38–44.
[9] H.S. Yin, R.G. Paterson, X. Wen, R.A. Lamb, T.S. Jardetzky, Structure of the uncleaved ectodomain of the paramyxovirus (hPIV3) fusion protein, Proc. Natl. Acad. Sci. U. S. A. 102 (2005) 9288–9293.
[10] D.C. Chan, D. Fass, J.M. Berger, P.S. Kim, Core structure of gp41 from the HIV envelope glycoprotein, Cell 89 (1997) 263–273.
[11] W. Weissenhorn, A. Dessen, S.C. Harrison, J.J. Skehel, D.C. Wiley, Atomic structure of the ectodomain from HIV-1 gp41, Nature 387 (1997) 426–430.
[12] Y.H. Kim, J.E. Donald, G. Grigoryan, G.P. Leser, A.Y. Fadeev, R.A. Lamb, W. F. DeGrado, Capture and imaging of a prehairpin fusion intermediate of the paramyxovirus PIV5, Proc. Natl. Acad. Sci. U. S. A. 108 (2011) 20992–20997.
[13] G. Frey, H. Peng, S. Rits-Volloch, M. Morelli, Y. Cheng, B. Chen, A fusion-intermediate state of HIV-1 gp41 targeted by broadly neutralizing antibodies, Proc. Natl. Acad. Sci. U. S. A. 105 (2008) 3739–3744.
[14] B. Kwon, M. Lee, A.J. Waring, M. Hong, Oligomeric structure and three-dimensional fold of the HIV gp41 membrane-proximal external region and transmembrane domain in phospholipid bilayers, J. Am. Chem. Soc. 140 (2018) 8246–8259.
[15] Q. Fu, M.M. Shaik, Y. Cai, F. Ghantous, A. Piai, H. Peng, S. Rits-Volloch, Z. Liu, S. C. Harrison, M.S. Seaman, B. Chen, J.J. Chou, Structure of the membrane proximal external region of HIV-1 envelope glycoprotein, Proc. Natl. Acad. Sci. U. S. A. 115 (2018) E8892–e8899.
[16] J. Dev, D. Park, Q. Fu, J. Chen, H.J. Ha, F. Ghantous, T. Herrmann, W. Chang, Z. Liu, G. Frey, M.S. Seaman, B. Chen, J.J. Chou, Structural basis for membrane anchoring of HIV-1 envelope spike, Science 353 (2016) 172–175.
[17] S.C. Chiliveri, J.M. Louis, R. Ghirlando, J.L. Baber, A. Bax, Tilted, uninterrupted, monomeric HIV-1 gp41 transmembrane helix from residual dipolar couplings, J. Am. Chem. Soc. 140 (2018) 34–37.
[18] M. Lee, C.A. Morgan, M. Hong, Fully hydrophobic HIV gp41 adopts a hemifusion-like conformation in phospholipid bilayers, J. Biol. Chem. 294 (2019) 14732–14744.
[19] H. Yao, M. Lee, S.Y. Liao, M. Hong, Solid-state nuclear magnetic resonance investigation of the structural topology and lipid interactions of a viral fusion protein chimera containing the fusion peptide and transmembrane domain, Biochemistry 55 (2016) 6787–6800.
[20] N.W. Schmidt, A. Mishra, G.H. Lai, M. Davis, L.K. Sanders, D. Tran, A. Garcia, K. P. Tai, P.B. McCray, A.J. Ouellette, M.E. Selsted, G.C. Wong, Criterion for amino acid composition of defensins and antimicrobial peptides based on geometry of membrane destabilization, J. Am. Chem. Soc. 133 (2011) 6720–6727.
[21] N.W. Schmidt, A. Mishra, J. Wang, W.F. DeGrado, G.C. Wong, Influenza virus a M2 protein generates negative Gaussian membrane curvature necessary for budding and scission, J. Am. Chem. Soc. 135 (2013) 13710–13719.
[22] H. Yao, M.W. Lee, A.J. Waring, G.C. Wong, M. Hong, Viral fusion protein transmembrane domain adopts beta-strand structure to facilitate membrane topological changes for virus-cell fusion, Proc. Natl. Acad. Sci. U. S. A. 112 (2015) 10926–10931.
[23] D.P. Siegel, R.M. Epand, Effect of influenza hemagglutinin fusion peptide on lamellar/inverted phase transitions in dipalmitoleoylphosphatidylethanolamine: implications for membrane fusion mechanisms, Biochim. Biophys. Acta 1468 (2000) 87–98.
[24] Y. Yang, H. Yao, M. Hong, Distinguishing bicontinuous lipid cubic phases from isotropic membrane morphologies using 31P solid-state NMR spectroscopy, J. Phys. Chem. 119 (2015) 4993–5001.
[25] M.K. Callahan, P.M. Popernack, S. Tsutsui, L. Truong, R.A. Schlegel, A. J. Henderson, Phosphatidylserine on HIV envelope is a cofactor for infection of monocytic cells, J. Immunol. 170 (2003) 4840–4845.
[26] E. Zaitseva, E. Zaitsev, K. Melikov, A. Arakelyan, M. Marin, R. Villasmil, L. B. Margolis, G.B. Melikyan, L.V. Chernomordik, Fusion stage of HIV-1 entry depends on virus-induced cell surface exposure of phosphatidylserine, Cell Host Microbe 22 (2017) 99–110.e117.
[27] Z.H. Liao, D.R. Graham, J.E.K. Hildreth, Lipid rafts and HIV pathogenesis: virion-associated cholesterol is required for fusion and infection of susceptible cells, Aids Res. Hum. Retrov. 19 (2003) 675–687.
[28] S.T. Yang, V. Kiessling, J.A. Simmons, J.M. White, L.K. Tamm, HIV gp41-mediated membrane fusion occurs at edges of cholesterol-rich lipid domains, Nat. Chem. Biol. 11 (2015) 424–431.
[29] G.C. Carter, L. Bernstone, D. Sangani, J.W. Bee, T. Harder, W. James, HIV entry in macrophages is dependent on intact lipid rafts, Virology 386 (2009) 192–202.
[30] M.K. Domanska, D. Wrona, P.M. Kasson, Multiphasic effects of cholesterol on influenza fusion kinetics reflect multiple mechanistic roles, Biophys. J. 105 (2013) 1383–1387.
[31] C.M. Gabrys, R. Yang, C.M. Wasniewski, J. Yang, C.G. Canlas, W. Qiang, Y. Sun, D. P. Weliky, Nuclear magnetic resonance evidence for retention of a lamellar membrane phase with curvature in the presence of large quantities of the HIV fusion peptide, Biochim. Biophys. Acta 1798 (2010) 194–201.
[32] B. Brügger, B. Glass, P. Haberkant, I. Leibrecht, F.T. Wieland, H.G. Krausslich, The HIV lipidome: a raft with an unusual composition, Proc. Natl. Acad. Sci. U. S. A. 103 (2006) 2641–2646.
[33] M. Lorizate, T. Sachsenheimer, B. Glass, A. Habermann, M.J. Gerl, H.G. Kräusslich, B. Brügger, Comparative lipidomics analysis of HIV-1 particles and their producer cell membrane in different cell lines, Cell. Microbiol. 15 (2013) 292–304.
[34] P. Zhu, E. Chertova, J. Bess Jr., J.D. Lifson, L.O. Arthur, J. Liu, K.A. Taylor, K. H. Roux, Electron tomography analysis of envelope glycoprotein trimers on HIV and simian immunodeficiency virus virions, Proc. Natl. Acad. Sci. U. S. A. 100 (2003) 15812–15817.
[35] D. Lingwood, K. Simons, Lipid rafts as a membrane-organizing principle, Science 327 (2010) 46–50.
[36] N.T. Back, L. Smit, M. Schutten, P.L. Nara, M. Tersmette, J. Goudsmit, Mutations in human immunodeficiency virus type 1 gp4l affect sensitivity to neutralization by gpl20 antibodies, J. Virol. 67 (1993) 6897–6902.
[37] M.D. Simon, P.L. Heider, A. Adamo, A.A. Vinogradov, S.K. Mong, X. Li, T. Berger, R.L. Policarpo, C. Zhang, Y. Zou, X. Liao, A.M. Spokoyny, K.F. Jensen, B. L. Pentelute, Rapid flow-based peptide synthesis, Chembiochem 15 (2014) 713–720.
[38] A.R. Grimmer, A. Kretschmer, V.B. Cajipe, Influence of magic angle spinning on sample temperature, Magn. Reson. Chem. 35 (1997) 86–90.
[39] A. Böckmann, C. Gardiennet, R. Verel, A. Hunkeler, A. Loquet, G. Pintacuda, L. Emsley, B.H. Meier, A. Lesage, Characterization of different water pools in solid-state NMR protein samples, J. Biomol. NMR 45 (2009) 319–327.
[40] K.K. Kumashiro, K. Schmidt-Rohr, O.J. Murphy, K.L. Ouellette, W.A. Cramer, L. K. Thompson, A novel tool for probing membrane protein structure: solid-state NMR with proton spin diffusion and X-nucleus detection, J. Am. Chem. Soc. 120 (1998) 5043–5051.
[41] R. Mani, J.J. Buffy, A.J. Waring, R.I. Lehrer, M. Hong, Solid-state NMR investigation of the selective disruption of lipid membranes by Protegrin-1, Biochemistry 43 (2004) 13839–13848.
[42] R. Mani, S.D. Cady, M. Tang, A.J. Waring, R.I. Lehrer, M. Hong, Membrane-dependent oligomeric structure and pore formation of a beta-hairpin antimicrobial peptide in lipid bilayers from solid-state NMR, Proc. Natl. Acad. Sci. U. S. A. 103 (2006) 16242–16247.
[43] G. van Meer, D.R. Voelker, G.W. Feigenson, Membrane lipids: where they are and how they behave, Nat. Rev. Mol. Cell Biol. 9 (2008) 112–124.
[44] K. Kastl, M. Menke, E. Lüthgens, S. Faiss, V. Gerke, A. Janshoff, C. Steinem, Partially reversible adsorption of annexin A1 on POPC/POPS bilayers investigated

by QCM measurements SFM, and DMC simulations, Chembiochem 7 (2006) 106–115.
[45] J.R. Silvius, J. Gagne, Calcium-induced fusion and lateral phase separations in phosphatidylcholine-phosphatidylserine vesicles. Correlation by calorimetric and fusion measurements, Biochemistry 23 (1984) 3241–3247.
[46] F. Lindström, P.T. Williamson, G. Gröbner, Molecular insight into the electrostatic membrane surface potential by 14n/31p MAS NMR spectroscopy: nociceptin-lipid association, J. Am. Chem. Soc. 127 (2005) 6610–6616.
[47] L.K. Tamm, J. Crane, V. Kiessling, Membrane fusion: a structural perspective on the interplay of lipids and proteins, Curr. Opin. Struct. Biol. 13 (2003) 453–466.
[48] R.P. Rand, Physical force considerations in model and biological membranes, Can. J. Biochem. Cell Biol 62 (1984) 752–775.
[49] K.S. Bruzik, G.M. Salamonczyk, B. Sobon, 13C CP-MAS study of the gel phases of 1,2-dipalmitoylphosphatidylcholine, Biochim. Biophys. Acta 1023 (1990) 143–146.
[50] J. Frye, A.D. Albert, B.S. Selinsky, P.L. Yeagle, Cross polarization P-31 nuclear magnetic resonance of phospholipids, Biophys. J. 48 (1985) 547–552.
[51] T. Doherty, M. Hong, 2D 1H–31P solid-state NMR studies of the dependence of inter-bilayer water dynamics on lipid headgroup structure and membrane peptides, J. Magn. Reson. 196 (2009) 39–47.
[52] D. Huster, K. Gawrisch, NOESY NMR crosspeaks between lipid headgroups and hydrocarbon chains: spin diffusion or molecular disorder? J. Am. Chem. Soc. 121 (1999) 1992–1993.
[53] S.E. Feller, C.A. Brown, D.T. Nizza, K. Gawrisch, Nuclear overhauser enhancement spectroscopy cross-relaxation rates and ethanol distribution across membranes, Biophys. J. 82 (2002) 1396–1404.
[54] H. Yao, M. Hong, Membrane-dependent conformation, dynamics, and lipid interactions of the fusion peptide of the paramyxovirus PIV5 from solid-state NMR, J. Mol. Biol. 425 (2013) 563–576.
[55] B. Kollmitzer, P. Heftberger, M. Rappolt, G. Pabst, Monolayer spontaneous curvature of raft-forming membrane lipids, Soft Matter 9 (2013) 10877–10884.
[56] B. Kwon, T. Mandal, M.R. Elkins, Y. Oh, Q. Cui, M. Hong, Cholesterol interaction with the trimeric HIV fusion protein gp41 in lipid bilayers investigated by solid-state NMR spectroscopy and molecular dynamics simulations, J. Mol. Biol. 432 (2020) 4705–4721.
[57] Z.H. Liao, L.M. Cimakasky, R. Hampton, D.H. Nguyen, J.E.K. Hildreth, Lipid rafts and HIV pathogenesis: host membrane cholesterol is required for infection by HIV type 1, Aids Res. Hum. Retrov. 17 (2001) 1009–1019.
[58] J.R. Silvius, Cholesterol modulation of lipid intermixing in phospholipid and glycosphingolipid mixtures. Evaluation using fluorescent lipid probes and brominated lipid quenchers, Biochemistry 31 (1992) 3398–3408.
[59] W.F. Zeno, A. Rystov, D.Y. Sasaki, S.H. Risbud, M.L. Longo, Crowding-induced mixing behavior of lipid bilayers: examination of mixing energy phase, packing geometry, and reversibility, Langmuir 32 (2016) 4688–4697.
[60] D. Huster, K. Arnold, K. Gawrisch, Influence of docosahexaenoic acid and cholesterol on lateral lipid organization in phospholipid mixtures, Biochemistry 37 (1998) 17299–17308.
[61] S.-T. Yang, V. Kiessling, L.K. Tamm, Line tension at lipid phase boundaries as driving force for HIV fusion peptide-mediated fusion, Nat. Commun. 7 (2016).
[62] M.R. Elkins, A. Bandara, G.A. Pantelopulos, J.E. Straub, M. Hong, Direct observation of cholesterol dimers and tetramers in lipid bilayers, J. Phys. Chem. B 125 (2021) 1825–1837.
[63] B. van Wilgenburg, M.D. Moore, W.S. James, S.A. Cowley, The productive entry pathway of HIV-1 in macrophages is dependent on endocytosis through lipid rafts containing CD4, PLoS One 9 (2014), e86071.
[64] T. Wang, S.D. Cady, M. Hong, NMR determination of protein partitioning into membrane domains with different curvatures and application to the influenza M2 peptide, Biophys. J. 102 (2012) 787–794.
[65] J.E. Donald, Y. Zhang, G. Fiorin, V. Carnevale, D.R. Slochower, F. Gai, M.L. Klein, W.F. DeGrado, Transmembrane orientation and possible role of the fusogenic peptide from parainfluenza virus 5 (PIV5) in promoting fusion, Proc. Natl. Acad. Sci. U. S. A. 108 (2011) 3958–3963.
[66] A. Piai, J. Dev, Q. Fu, J.J. Chou, Stability and water accessibility of the trimeric membrane anchors of the HIV-1 envelope spikes, J. Am. Chem. Soc. 139 (2017) 18432–18435.
[67] M.K. Baker, V.K. Gangupomu, C.F. Abrams, Characterization of the water defect at the HIV-1 gp41 membrane spanning domain in bilayers with and without cholesterol using molecular simulations, Biochim. Biophys. Acta 1838 (2014) 1396–1405.
[68] H. Yao, M. Hong, Conformation and lipid interaction of the fusion peptide of the paramyxovirus PIV5 in anionic and negative-curvature membranes from solid-state NMR, J. Am. Chem. Soc. 136 (2014) 2611–2624.